THE JOURNAL OF PHYSICAL CHEMISTRY A
A JOURNAL OF THE AMERICAN CHEMICAL SOCIETY

pubs.acs.org/JPCA
Article

The Remarkable I_2O_3 Molecule: A New View from Theory

Published as part of The Journal of Physical Chemistry A special issue "Michael A. Duncan Festschrift".

Carson L. Tang, Justin M. Turney, and Henry F. Schaefer, III*

Cite This: J. Phys. Chem. A 2025, 129, 7507−7516
Read Online

ABSTRACT: Atmospheric iodine chemistry has garnered increasing attention as a result of increased iodine emissions. A key subset of this chemistry involves iodine oxides (I_2O_{2-5}), which serve as precursors to particle formation. Among these, I_2O_3 is the simplest iodine oxide involved in particle formation, but it has remained undetected in the atmosphere. Previous theoretical studies have characterized this peculiar molecule, primarily using energies to refine geometries obtained at low levels of theory. Due to the reemerging interest in I_2O_3, this study presents geometries optimized at the CCSD(T)/aug-cc-pwCVTZ-PP level of theory—marking the first instance, to the best of our knowledge, where this system has been studied exclusively with CCSD(T). Harmonic vibrational frequencies were computed at the same level of theory. Final energetics were obtained using the very high level CCSDT(Q) method with basis sets up to quintuple-zeta cardinality (aug-cc-pwCV5Z-PP) and extrapolated to the CBS limit to yield CCSDT(Q)/CBS//CCSD(T)/aug-cc-pwCVTZ-PP energies. These energies include harmonic zero-point vibrational energy corrections and scalar relativistic energy corrections. Additionally, this study discovers new isomers along the I_2O_3 potential energy surface, a novel contribution to the field. The performance of different computational methods and DFT functionals commonly used in atmospheric chemistry is also assessed relative to high-level theoretical methods.

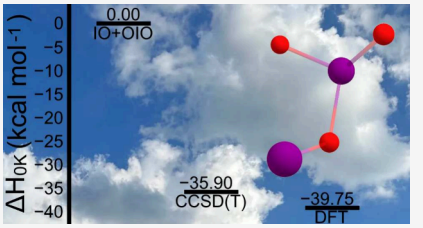

INTRODUCTION

Aerosols in the atmosphere have been shown to impact the Earth−atmosphere system, showing effects on air quality, human health, weather, and climate.[1] Aerosols also act as cloud condensation nuclei (CCN), which have been hypothesized to accelerate the melting of sea ice.[1,2] Given their significant role in the atmosphere, understanding how these particles are formed is crucial. A major source of these particles is the result of new particle formation (NPF), which accounts for approximately 50% of CCN in the Earth's atmosphere. NPF begins with the formation of clusters in the gas phase, which grow in size as they collide with surrounding clusters.[1] The most prevalent nucleating species has historically been sulfuric acid, due to its low vapor pressure under typical atmospheric conditions, in addition to its ability to form hydrogen bonds with many important compounds in the atmosphere.[1,3] Additional nucleating precursors reported in the literature include: ammonia/amines, highly oxygenated molecules, organic compounds, iodine oxides, and iodine oxyacids.[1,4−7] However, uncertainties remain regarding the mechanisms of NPF and the chemical species involved. Available NPF data come from field measurements, laboratory experiments, and theoretical studies, but these results are often conflicting. While theoretical work in this field has been relatively rare, it has been advocated as a valuable complement to field measurements and experimental results.[1] Iodine oxyacids, such as HIO_3 and HIO_2, have been proposed to be the main drivers in NPF.[5−7] One possible pathway for the formation of these oxyacids is the reaction of iodine oxides with water.[8] Therefore, understanding the properties and behavior of iodine oxides is just as important as studying the iodine oxyacids themselves.

Iodine oxides are the most obscure of the nucleating species mentioned above. The atmospheric chemistry of iodine has gained increasing importance, as evidenced by the abundance of references to the review by Saiz-Lopez et al. in 2011.[9] Atmospheric iodine-containing species in general have risen in concentrations since the 1950s, a result of rising ozone (O_3) levels from both natural and anthropogenic sources.[3,7,10−13] Seaweeds and algae in coastal waters emit diatomic iodine (I_2) and organoiodine compounds (e.g., CH_3I) into the atmosphere, photochemically producing the iodine radical ($I^\bullet$).[9,10] Ozone in the atmosphere then reacts with $I^\bullet$ to produce iodine monoxide (IO) and iodine dioxide (IO_2).[9,10] As described in the influential review by Saiz-Lopez et al., higher-order iodine oxides (I_2O_{2-5}) are produced from a series of self-reactions between IO and OIO.[9] The simplest iodine oxide that directly leads to particle formation is I_2O_3, a species frequently noted but not well characterized.[2−4,10,14−93]

Received: June 20, 2025
Revised: July 25, 2025
Accepted: July 29, 2025
Published: August 4, 2025

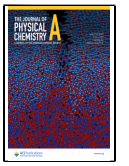

Kaltsoyannis and Plane performed early quantum chemical calculations on I_2O_3 as part of a study of important iodine containing compounds in the atmosphere in 2008.[89] At the CCSD(T)/aug-cc-pVTZ//B3LYP/aug-cc-pVTZ level of theory, they concluded that I_2O_3 is a very stable molecule with C_1 symmetry.[89] They also reported harmonic vibrational frequencies, but did not include the intensities or symmetries of the vibrational modes. In 2013, a combined experimental (Gómez Martín et al.) and theoretical (Gálvez et al.) study provided the first direct experimental evidence of I_2O_3 in the gas phase.[90,91] The theoretical portion of this study reported CCSD(T) energies computed on MP2 or B3LYP geometries.[90] However, Gálvez et al. only report bond lengths of I_2O_3, omitting bond angles and harmonic frequencies.[90] Gómez Martín et al. conducted another combined experimental and theoretical study in 2020 to explain atmospheric particle formation through clustering of iodine oxides.[92] This study included a potential energy surface for the reaction of I_2O_3 with water, calculated at the CCSD(T)/aug-cc-pVTZ +LAN2LDZ//M06-2X/aug-cc-pVDZ+LANL2DZ level of theory.[92] More recently, in the latter half of 2024, Ning et al. presented a study on the heterogeneous chemistry of I_2O_3, including molecular dynamics simulations and quantum chemical calculations of I_2O_3 at the DLPNO-CCSD(T)/aug-cc-pVTZ(-PP)//M06-2X/aug-cc-pVTZ(-PP) level of theory.[93] Engsvang, Wu, and Elm recently conducted a computational benchmark of iodine oxyacid and oxide dimers.[94] While this benchmark only included I_2O_4 and I_2O_5, the title suggests a future benchmark that may include I_2O_3. They found that optimizing structures at the ωB97X-D3BJ/aug-cc-pVTZ-PP or M06-2X/aug-cc-pVTZ-PP level of theory achieved the best thermal contribution to the binding free energy.[94] Electronic energy corrections were computed using the ZORA-DLPNO-CCSD(T_0) method with the SARC-ZORA-TZVPP basis set for iodine and the ma-ZORA-def2-TZVPP basis set for noniodine atoms.[94]

Despite experimental observations, the structure and infrared spectrum of I_2O_3 have yet to be reported. Field measurements have thus far failed to detect I_2O_3 in the atmosphere. This may be due to I_2O_3 being considered a "dead end" in the current understanding of iodine chemistry in the atmosphere.[93] However, recent studies have shown continued interest in this peculiar system and atmospheric iodine chemistry in general.[4,10,92−94] For example, recent work by Francisco and co-workers highlights that I_2O_3 plays a critical role in the ocean−atmosphere iodine cycle.[93]

Previous theoretical works report CCSD(T) or DLPNO-CCSD(T) energies on geometries optimized at lower levels of theory (e.g., DFT).[89,90,92,93] In the present study, I_2O_3 has been fully optimized using the CCSD(T) method. With these structures, much higher levels of theory have been applied to I_2O_3. The results will be compared with other *ab initio* methods and various DFT functionals commonly seen in atmospheric chemistry. Additional isomers on the potential energy surface are also presented. To the best of our knowledge, this is the first study to optimize I_2O_3 with the CCSD(T) method and to present additional minima along the PES, regardless of the level of theory.

COMPUTATIONAL METHODS

Here, computations were performed using a variety of post-Hartree−Fock methods and, for comparison, DFT functionals. Geometry optimization and harmonic vibrational frequency evaluations for the I_2O_3 isomer lowest in energy were carried out with the MP2, CCSD, and CCSD(T) methods.[95−108] Functionals frequently used in atmospheric chemistry were also employed to assess their performance in predicting geometric parameters and vibrational frequencies against the gold standard CCSD(T).[3] These functionals include M06-2X, PW91, ωB97X-D, and the familiar B3LYP.[109−112] In the present research, six different basis set combinations were used to assess basis set dependence as well. The first combination employed the cc-pVXZ (X = D, T) basis sets for oxygen atoms and the cc-pVXZ-PP basis sets for iodine atoms, and will be abbreviated as XZ.[113−119] The second combination used the aug-cc-pVXZ basis sets for oxygen atoms and aug-cc-pVXZ-PP basis sets for iodine atoms, abbreviated as AVXZ.[113−116,120,121] The third combination still used the aug-cc-pVXZ basis sets for oxygen atoms but utilized the larger aug-cc-pwCVXZ-PP basis sets for iodine atoms, abbreviated as ACVXZ.[113−116,120,121] This combination was suggested by Peterson, who noted that additional tight functions are essential for determining accurate structures and energetics for IO and OIO.[122] The structures and harmonic vibrational frequencies of the reactants that form I_2O_3, IO and OIO, in addition to the higher energy I_2O_3 isomers, were also computed but only at the CCSD(T)/ACVTZ level of theory. For the basis sets used within this study, the -PP appended to the end of a basis set refers to a relativistic effective core potential (ECP) that replaces the 28-electron core of the iodine atom. This is described by the noble gas configuration $[Ar]4s^23d^8$ and used to reduce the number of explicitly correlated electrons from 53 to 25.

Post-Hartree−Fock calculations for all the I_2O_3 isomers were computed with CFOUR version 2.1 with the NCC module.[123] Post-Hartree−Fock calculations for IO and OIO were computed with the VCC module of CFOUR, using an ROHF reference function. Unless otherwise noted, all post-Hartree−Fock computations were obtained from CFOUR. All DFT calculations were computed using Psi4 version 1.9 using an ultrafine grid.[124−127] In all cases, geometries were converged to an RMS gradient below 10^{-8} hartree $bohr^{-1}$. The Hartree−Fock and coupled cluster amplitude equations were also converged to 10^{-10} hartrees. Harmonic vibrational frequencies were obtained by finite differences of analytic gradients, following each geometry optimization to confirm that the final structure was a minimum along the potential energy surface. Anharmonic frequencies were computed for the global minimum with VPT2 using CFOUR.[128]

Electronic energies for each stationary point along the potential energy surface were computed using the focal point approach at the geometries obtained at the highest level of theory, CCSD(T)/ACVTZ.[129−132] Basis sets up to quintuple-zeta cardinality were used (O: aug-cc-pVXZ; I: aug-cc-pwCVXZ-PP, X = D, T, Q, 5) for Hartree−Fock, MP2, CCSD, and CCSD(T) energies, computed with the 2022 version of Molpro for the I_2O_3 isomers, IO, and OIO.[133−135] The energies obtained were extrapolated to the complete basis set limit using a three-point fitting equation for the Hartree−Fock energies and a two-point fitting equation for the correlation energies:

$$E_{HF} = A + Be^{-CX} \quad (1)$$

$$E_{corr} = A + BX^{-3} \quad (2)$$

Additional corrections were then appended to the resulting net energies to determine relative energies at 0 K. These

https://doi.org/10.1021/acs.jpca.5c04243
J. Phys. Chem. A 2025, 129, 7507−7516

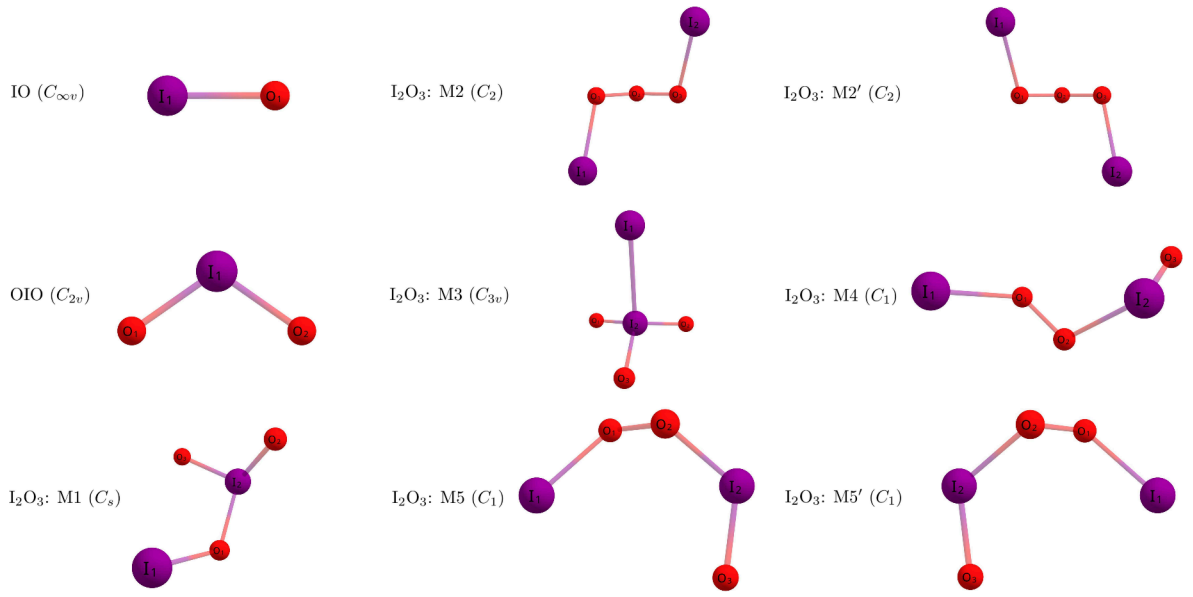

Figure 1. Qualitative geometries of IO, OIO, and I_2O_3 structures obtained at the CCSD(T)/aug-cc-pwCVTZ-PP level of theory.

corrections include a CCSDT correction (δ_T), a CCSDT(Q) correction ($\delta_{(Q)}$), a harmonic zero-point vibrational energy correction (δ_{ZPVE}), a scalar relativistic energy correction (δ_{rel}), and a spin-orbit correction (δ_{SO}).[136−141]

The CCSDT corrections were obtained at the CCSDT/ACVDZ level of theory using CFOUR for the I_2O_3 isomers and MRCC for IO and OIO.[142,143] The CCSDT(Q) corrections were obtained at the CCSDT(Q)/DZ level of theory using MRCC for all minima. For the open-shell species, the CCSDT(Q)/B energy was used.[144] The zero-point vibrational energy corrections were obtained from the harmonic vibrational frequency computations. Relativistic energy corrections were computed at the scalar level, without the inclusion of spin−orbit coupling. These energy corrections were computed with the X2C1E treatment in CFOUR, using the seg-cc-pVTZ-X2C basis set for oxygen atoms and the seg-cc-pwCVTZ-X2C basis set for iodine atoms.[145−152] Spin−orbit effects were treated with the internally contracted multireference configuration method in Molpro with a cc-pVTZ-DK basis set on all atoms. The active space configurations were defined as (7,4) for IO, full valence for OIO, and (6,6) for I_2O_3. By appending these additional corrections to the net energies obtained from the focal point approach, relative energies are given by the following:

$$\Delta_f H_0 = \Delta E_{CCSD(T)/CBS} + \delta_T + \delta_{(Q)} + \delta_{ZPVE} + \delta_{rel} + \delta_{SO} \quad (3)$$

RESULTS AND DISCUSSION

Geometries. Shown in Figure 1 are the qualitative geometries of the IO, OIO, and I_2O_3 structures obtained at the CCSD(T)/ACVTZ level of theory. The isomer labeled as M1, located on the bottom left of Figure 1, is the global minimum that has been considered in previous reports. To the best of our knowledge, the additional I_2O_3 isomers (M2−M5) have not been reported until now. These additional structures were identified by examining the potential energy surfaces of their corresponding lighter halogen analogs (Y_2O_3, Y = F, Cl, Br).[153−158] Notably, isomers M2 and M5 are enantiomers of M2′ and M5′, respectively. They share the same bond lengths, same vibrational modes, and are isoenergetic with each other. The present study focuses primarily on the M1 isomer, which is shown isolated in Figure 2. Geometric parameters for IO, OIO, and the additional I_2O_3 structures are shown in the Supporting Information.

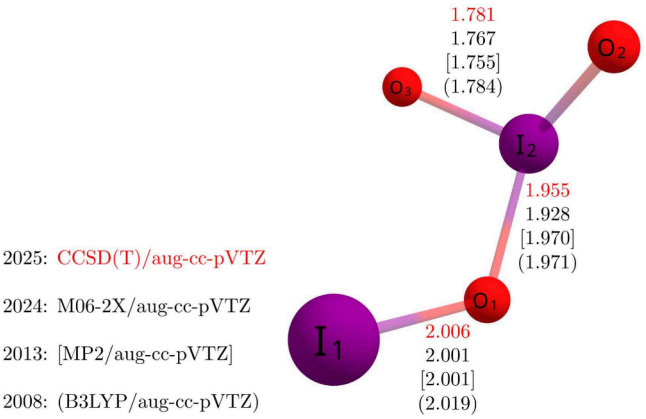

Figure 2. Predicted values of the I_2O_3 bond lengths (Å) at the CCSD(T)/aug-cc-pVTZ-PP level of theory (shown in red) compared to values previously reported in the literature from different methods.[89,90,93] Point group: C_s. See the text for different ECPs used.

In Figure 2, bond lengths of the M1 isomer obtained in this study at the CCSD(T)/AVTZ level of theory are displayed in red print. For comparison, previously reported bond lengths obtained using M06-2X, MP2, and B3LYP, all with the same aug-cc-pVTZ basis sets, are shown in black with square brackets and parentheses.[89,90,92] All bond lengths are reported in angstroms. While there is some variation between the four sets of values shown, none match the CCSD(T) results closely. However, certain values, such as the I_2-O_3 bond length, differ by only 0.003 Å. These variations may in part be attributed to differences in the effective core potentials (ECPs) used for iodine in the various studies. For instance, Kaltsoyannis and Plane (2008) used Glukhovstev's all-electron iodine basis set, while Gálvez et al. (2013) employed an ECP replacing the 46-

https://doi.org/10.1021/acs.jpca.5c04243
J. Phys. Chem. A 2025, 129, 7507−7516

electron core of iodine. The present study uses the same Peterson ECP as Francisco and co-workers, which replaces the 28-electron core of iodine.[121] Benchmark studies of ECPs have demonstrated that outer-core electrons play an important role in accurately determining bond lengths and related properties.[121]

To provide a consistent comparison, our study presents bond lengths, bond angles, and dihedral angles computed using identical basis sets and ECPs across all methods and DFT functionals. The results are tabulated in the Supporting Information, showing raw geometric values and values relative to CCSD(T) results since there are currently no experimental data. These tables include data from seven methods: B3LYP, M06-2X, PW91, ωB97X-D, MP2, CCSD, and CCSD(T). Each method was used with six basis set combinations: DZ, AVDZ, ACVDZ, TZ, AVTZ, and ACVTZ, yielding a total of 42 levels of theory.

For this study, small deviations were defined as bond length differences less than 0.01 Å and bond angle or dihedral deviations of less than 1°. Based on our results, B3LYP and MP2 performed the best while CCSD and PW91 performed the worst in predicting geometries compared to CCSD(T). Specifically, B3LYP and MP2 yielded 27/42 (64.3%) and 26/42 (61.9%) values that had smaller deviations, respectively. The CCSD and PW91 methods, yielded 17/42 (40.5%) and 16/42 (38.1%) values with small deviations, respectively. From our results, mean absolute errors (MAE), root-mean-square errors (RMSE), and maximum errors were determined for bond lengths and bond angles to see how each method performed in comparison to CCSD(T). These values are shown in Table 1.

Table 1. Performance of Different Methods in Predicting Equilibrium Geometries Relative to CCSD(T) Shown by Mean Absolute Error, Root-Mean-Square Error, and Maximum Error

	Bond Lengths (Å)			Bond Angles (deg)		
	MAE	RMSE	Max. Error	MAE	RMSE	Max. Error
MP2	0.016	0.019	0.035	0.8	1.2	2.6
CCSD	0.025	0.028	0.048	0.8	1.2	2.8
B3LYP	0.012	0.015	0.034	1.3	2.0	4.5
M06-2X	0.027	0.031	0.058	0.9	1.2	3.0
PW91	0.032	0.041	0.080	0.8	1.0	1.7
ωB97X-D	0.015	0.018	0.034	1.6	2.5	6.1

Based on the values in Table 1, B3LYP is the method that predicts bond lengths closest to CCSD(T) while PW91 is the method that predicts bond angles and dihedrals closest to CCSD(T). Interestingly, while PW91 is able to predict bond angles, it performs the worst in predicting bond lengths. In predicting equilibrium geometries as a whole, it would seem MP2 is the method that is able to predict geometries closest to CCSD(T) quality. As for DFT functionals, B3LYP is likely the best choice, having the smallest errors in bond lengths and reasonable errors for bond angles.

Energetics. To determine relative energies, I_2O_3 is described relative to the reactants by the focal point table shown by Table 2.[129−132] The energy is still changing by the time CCSD(T) is introduced, with a subsequent change of 1.29 kcal mol^{-1}. This raises a concern for multireference character in the system. Inspection of diagnostics such as T_1 and T_2 amplitudes however, presented no major multireference character. Higher order methods such as CCSDT and CCSDT(Q) were used to address this concern. The full CCSDT correction is still high with a change of 1.05 kcal mol^{-1}. The CCSDT(Q) correction is within chemical accuracy (1 kcal mol^{-1}), but is still not as converged as one would hope with CCSDT(Q), with a change of 0.61 kcal mol^{-1}. It would seem that even higher order methods such as CCSDTQ or CCSDTQ(P) may be needed to precisely converge the energy of this system. The total relativistic correction of 8.20 kcal mol^{-1} is the largest correction. However, this large change does not seem too alarming as previous studies have stated that inclusion of relativistic effects may cause the relative energy to increase.[89,159] The focal point tables of the other I_2O_3 isomers can be found in the Supporting Information. Figure 3 shows the energies of all I_2O_3 isomers relative to the reactants.

Table 2. Incremental Focal Point Table for the M1 Isomer Relative to the Reactants, IO and OIO; The Final Relative Energy Is Obtained as $\Delta_f H_0 = \Delta E_{CCSD(T)/CBS} + \delta_T + \delta_{(Q)} + \delta_{ZPVE} + \delta_{rel} + \delta_{SO}$

Basis Set	RHF	$+\delta_{MP2}$	$+\delta_{CCSD}$	$+\delta_{(T)}$	Net
DZ	−20.11	−22.72	+9.04	−1.29	−35.07
TZ	−26.93	−25.91	+10.32	−1.40	−43.92
QZ	−27.78	−26.47	+10.13	−1.44	−45.56
5Z	−27.82	−26.89	+10.09	−1.47	−46.09
CBS	[−27.78]	[−26.87]	[+9.99]	[−1.47]	[−46.13]

$\Delta_f H_0$ = −46.13 + 1.05 − 0.61 + 1.59 + 7.20 + 1.00 = −35.90 ± 0.08 kcal mol^{-1}

The final energy reported by Kaltsoyannis and Plane was −39.75 kcal mol^{-1}, nearly 4 kcal mol^{-1} different from the present research. Kaltsoyannis and Plane obtained their result using CCSD(T) energies:

$$E(\text{total}) = E(I_2O_3) - E(\text{OIO} + \text{IO}) + \delta_{ZPVE} + \delta_{soc} \quad (4)$$

where δ_{ZPVE} is a zero-point energy correction and δ_{soc} is a spin−orbit coupling correction.

The possibility of additional I_2O_3 isomers undergoing rearrangement to the global minimum is an intriguing consideration. The M2 and M3 isomers do not appear to have a straightforward pathway for rearrangement. However, the M4 and M5 isomers may be able to rearrange to the global minimum. Since the M4 and M5 isomers are isoenergetic and share very similar geometric parameters, the M5 isomer will be the focus of the following discussion. Notably, the M5 isomer also appears on the Cl_2O_3 potential energy surface reported by Zhu and Lin.[154] Their surface is highly detailed, connecting six minima through 10 different transition states. On this surface, the Cl_2O_3 analog of the M5 isomer presented here can be connected to four different transition states. Two of those are particularly relevant: one connects the Cl_2O_3 analogs of the M1 and M5 isomers from this study, while the other connects the M5 analog to its reactants, ClO and OClO. Based on this, it may be possible for the I_2O_3 M5 isomer to undergo rearrangement to the M1 global minimum. However, further investigation into the transition states connecting the minima identified here would be needed to confirm this.

Vibrational Frequencies. The vibrational frequencies of I_2O_3 have not been reported experimentally. The only available theoretical values are from Kaltsoyannis and Plane, calculated at the B3LYP/AVTZ level of theory.[89] However, their computations were performed in C_1 symmetry and did not include infrared intensity predictions. Table 3 presents

https://doi.org/10.1021/acs.jpca.5c04243
J. Phys. Chem. A 2025, 129, 7507−7516

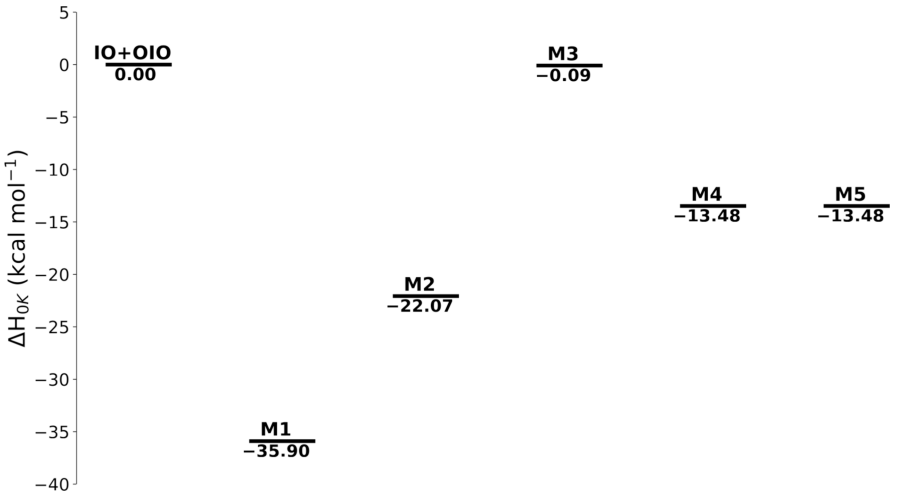

Figure 3. Energies of the I_2O_3 isomers from this study, in kcal mol^{-1}, shown relative to the reactants.

Table 3. Vibrational Frequencies (cm^{-1}), Infrared Intensities (km mol^{-1}), and Symmetries of the Vibrational Modes of I_2O_3 Computed in This Study[a]

	CCSD(T)/ACVTZ**	CCSD(T)/ACVTZ	CCSD(T)/AVTZ	B3LYP/AVTZ	B3LYP/AVTZ*
ω_1	34 (6, a″)	35 (6, a″)	32 (6, a″)	25 (5, a″)	43.4 (a)
ω_2	97 (5, a′)	97 (5, a′)	96 (5, a′)	85 (4, a′)	88.2 (a)
ω_3	239 (7, a″)	242 (7, a″)	236 (8, a″)	225 (7, a″)	236.8 (a)
ω_4	256 (24, a′)	258 (24, a′)	253 (24, a′)	246 (24, a′)	254.6 (a)
ω_5	301 (15, a′)	302 (15, a′)	294 (17, a′)	277 (16, a′)	297.5 (a)
ω_6	467 (26, a′)	464 (27, a′)	466 (26, a′)	433 (30, a′)	442.5 (a)
ω_7	638 (142, a′)	651 (156, a′)	653 (153, a′)	608 (102, a′)	625.7 (a)
ω_8	861 (25, a′)	871 (25, a′)	872 (25, a′)	851 (35, a′)	872.7 (a)
ω_9	890 (79, a″)	900 (83, a″)	902 (82, a″)	875 (92, a″)	901.2 (a)

[a]Unless otherwise noted, the vibrational frequencies were obtained using a harmonic approximation. The values for CCSD(T)/ACVTZ**, noted with a double asterisk, were obtained using VPT2. The values for B3LYP/AVTZ*, noted with an asterisk, are from Kaltsoyannis and Plane.[89]

anharmonic and harmonic vibrational frequencies computed in this study with the CCSD(T)/ACVTZ, CCSD(T)/AVTZ, and B3LYP/AVTZ methods, alongside the previously reported B3LYP/AVTZ values from Kaltsoyannis and Plane. Harmonic vibrational frequencies of IO, OIO, and the additional I_2O_3 isomers are shown in the Supporting Information.

In Table 3, the largest difference between the anharmonic and harmonic frequencies is 13 cm^{-1}. The largest difference between the anharmonic and harmonic intensities is only 6 km mol^{-1}. Given the small differences between the anharmonic and harmonic results, the harmonic frequencies appear to be sufficient.

Discrepancies exist between the B3LYP harmonic vibrational frequencies obtained by Kaltsoyannis and Plane and those predicted in this study. Specifically, the B3LYP frequencies reported by Kaltsoyannis and Plane are slightly higher, ranging from 3 to 25 cm^{-1} higher.[89] These B3LYP differences can likely be attributed to two factors. First, Kaltsoyannis and Plane employed a small all-electron basis set for iodine, whereas the present study utilized a 28-electron ECP with a better basis set. Second, their calculations were performed using the Amsterdam Density Functional (ADF) code, which employs Slater-type orbitals, in contrast to the Gaussian-type orbitals used in the codes for this study.

As with the geometric parameters, various method and basis set combinations were tested to evaluate their performance in predicting harmonic vibrational frequencies compared to CCSD(T). These results are tabulated in the Supporting Information. Across all the methods, PW91 performs the worst due to consistently producing an imaginary vibrational mode for the global minimum. Similar to the findings for geometric parameters, B3LYP yields values closest to those of CCSD(T). For double-ζ-quality basis sets, B3LYP outperforms MP2. However, with triple-ζ-quality basis sets, MP2 outperforms B3LYP for the lower frequency modes (ω_{1-7}). For the higher frequency modes (ω_8 and ω_9), MP2 tends to overestimates the values, whereas B3LYP produces results closer to CCSD(T).

From our results, mean absolute errors (MAE), root mean squared errors (RMSE), and maximum errors were determined for the harmonic vibrational frequencies to see how each method performed in comparison to CCSD(T). When computing these metrics, imaginary ω_1 values were omitted. These values are shown in Table 4. Similar to the geometric parameters, B3LYP is able to predict values closest to CCSD(T). Surprisingly, MP2 performs the worst when considering these statistical metrics. This is likely due to the overestimation of the higher frequency modes mentioned above.

CONCLUSIONS

The study focuses on the lowest energy I_2O_3 isomer, referred to as M1, and evaluates the performace of various computational methods and DFT functionals in comparison to CCSD(T). To our knowledge, additional I_2O_3 structures are discovered here for the first time. Some discrepancies in the geometric parameters of the M1 isomer are observed when

https://doi.org/10.1021/acs.jpca.5c04243
J. Phys. Chem. A 2025, 129, 7507−7516

Table 4. Performance of Different Methods in Predicting Harmonic Vibrational Frequencies (cm^{-1}) Relative to CCSD(T) as Shown by Mean Absolute Error, Root-Mean-Square Error, and Maximum Error

	MAE	RMSE	Max. Error
MP2	33	59	195
CCSD	23	27	58
B3LYP	13	16	44
M06-2X	33	40	77
PW91	36	42	99
ωB97X-D	20	27	82

comparing this study's results to three previous studies.[89,90,93] These differences are likely due to three key factors. First, one study employed ADF which uses Slater-type orbitals and allows relativistic effects to be incorporated when using DFT.[89] Second, the same study utilized an all-electron basis set for iodine atoms, whereas all other studies, including this one, used an ECP for iodine. Third, different studies employed varying ECPs; one used a 48-electron ECP, while this study and another used 28-electron ECPs.

When computing the energy of the M1 isomer relative to the reactants (IO and OIO), it was found that at the CCSD(T)/CBS level of theory, the system lies −35.90 kcal mol^{-1} lower in energy with the inclusion of additional energy corrections. This is nearly 4 kcal mol^{-1} higher than the previously reported theoretical value of −39.75 kcal mol^{-1}.[89]

When methods were standardized using consistent basis set and ECP combinations, B3LYP and MP2 were found to perform best in predicting geometric parameters relative to CCSD(T). Of these, B3LYP slightly outperformed MP2, although MP2 remains a strong choice for avoiding DFT. Conversely, PW91 and CCSD showed the poorest performance.

In predicting harmonic vibrational frequencies, PW91 consistently produced an imaginary vibrational mode across all six basis set combinations. Similar to the geometry predictions, B3LYP performed the best overall. Specifically, B3LYP excelled when using double-ζ-quality basis sets, whereas MP2 performed better with triple-ζ basis sets for the lower-frequency modes (ω_{1-7}). For higher-frequency modes (ω_8 and ω_9), MP2 tended to overestimate frequencies, while B3LYP produced results closer to CCSD(T).

Aside from B3LYP, the DFT methods that were included in this study were chosen because they are often mentioned in the literature to accurately predict equilibrium geometries of atmospheric clusters.[3,159] B3LYP was found to not only be the best performing functional, but best performing method, when considering the values presented in Tables 1 and 4 relative to CCSD(T). As there are currently no experimental results for the structure of I_2O_3 and given the renewed interest in these types of iodine species, B3LYP appears to be the best choice for future studies if CCSD(T) becomes too computationally expensive as the system size grows larger.

■ ASSOCIATED CONTENT

Supporting Information

The Supporting Information is available free of charge at https://pubs.acs.org/doi/10.1021/acs.jpca.5c04243.

Geometric parameters, harmonic vibrational frequencies, and focal point tables of the reactants (IO and OIO) and I_2O_3 structures (PDF)

■ AUTHOR INFORMATION

Corresponding Author

Henry F. Schaefer, III − *Center for Computational Quantum Chemistry, Department of Chemistry, University of Georgia, Athens, Georgia 30602, United States;* orcid.org/0000-0003-0252-2083; Phone: +1 (706) 542-2626; Email: ccq@uga.edu; Fax: +1 (706) 542-9454

Authors

Carson L. Tang − *Center for Computational Quantum Chemistry, Department of Chemistry, University of Georgia, Athens, Georgia 30602, United States;* orcid.org/0009-0002-2769-0796

Justin M. Turney − *Center for Computational Quantum Chemistry, Department of Chemistry, University of Georgia, Athens, Georgia 30602, United States*

Complete contact information is available at: https://pubs.acs.org/10.1021/acs.jpca.5c04243

Notes

The authors declare no competing financial interest.

■ ACKNOWLEDGMENTS

HFS thanks Professor Michael Duncan for collaboration, friendship, and a great many scientific discussions. This research was supported by the U.S. Department of Energy, Basic Energy Sciences, Division of Chemistry, Computational and Theoretical Chemistry (CTC) Program, under Contract DE-SC0018412.

■ REFERENCES

(1) Lee, S.-H.; Gordon, H.; Yu, H.; Lehtipalo, K.; Haley, R.; Li, Y.; Zhang, R. New Particle Formation in the Atmosphere: From Molecular Clusters to Global Climate. *J. Geophys. Res.* **2019**, *124*, 7098−7146.

(2) Gómez Martín, J. C.; Lewis, T. R.; James, A. D.; Saiz-Lopez, A.; Plane, J. M. C. Insights into the Chemistry of Iodine New Particle Formation: The Role of Iodine Oxides and the Source of Iodic Acid. *J. Am. Chem. Soc.* **2022**, *144*, 9240−9253.

(3) Zhang, X.; Tan, S.; Chen, X.; Yin, S. Computational chemistry of cluster: Understanding the mechanism of atmospheric new particle formation at the molecular level. *Chemosphere* **2022**, *308*, No. 136109.

(4) Finkenzeller, H.; Iyer, S.; He, X.-C.; Simon, M.; Koenig, T. K.; Lee, C. F.; Valiev, R.; Hofbauer, V.; Amorim, A.; Baalbaki, R.; et al. The gas-phase formation mechanism of iodic acid as an atmospheric aerosol source. *Nat. Chem.* **2023**, *15*, 129−135.

(5) Zhang, R.; Xie, H.-B.; Ma, F.; Chen, J.; Iyer, S.; Simon, M.; Heinritzi, M.; Shen, J.; Tham, Y. J.; Kurtén, T.; et al. Critical Role of Iodous Acid in Neutral Iodine Oxoacid Nucleation. *Environ. Sci. Technol.* **2022**, *56*, 14166−14177.

(6) Zhang, Y.; Li, D.; He, X.-C.; Nie, W.; Deng, C.; Cai, R.; Liu, Y.; Guo, Y.; Liu, C.; Li, Y.; et al. Iodine oxoacids and their roles in sub-3 nm particle growth in polluted urban environments. *Atmos. Chem. Phys.* **2024**, *24*, 1873−1893.

(7) He, X.-C.; Tham, Y. J.; Dada, L.; Wang, M.; Finkenzeller, H.; Stolzenburg, D.; Iyer, S.; Simon, M.; Kürten, A.; Shen, J.; et al. Role of iodine oxoacids in atmospheric aerosol nucleation. *Science* **2021**, *371*, 589−595.

(8) Xia, D.; Chen, J.; Yu, H.; Xie, H.-b.; Wang, Y.; Wang, Z.; Xu, T.; Allen, D. T. Formation Mechanisms of Iodine−Ammonia Clusters in Polluted Coastal Areas Unveiled by Thermodynamics and Kinetic Simulations. *Environ. Sci. Technol.* **2020**, *54*, 9235−9242.

(9) Saiz-Lopez, A.; Plane, J. M. C.; Baker, A. R.; Carpenter, L. J.; Von Glasow, R.; Gómez Martín, J. C.; McFiggans, G.; Saunders, R. W. Atmospheric Chemistry of Iodine. *Chem. Rev.* **2012**, *112*, 1773−1804.

(10) Xia, D.; Chen, J.; Yu, H.; Xie, H.-B.; Wang, Y.; Wang, Z.; Xu, T.; Allen, D. T. Formation Mechanisms of Iodine−Ammonia Clusters in Polluted Coastal Areas Unveiled by Thermodynamics and Kinetic Simulations. *Environ. Sci. Technol.* **2020**, *54*, 9235−9242.
(11) Cuevas, C. A.; Maffezzoli, N.; Corella, J. P.; Spolaor, A.; Vallelonga, P.; Kjær, H. A.; Simonsen, M.; Winstrup, M.; Vinther, B.; Horvat, C.; et al. Rapid increase in atmospheric iodine levels in the North Atlantic since the mid-20th century. *Nat. Commun.* **2018**, *9*, No. 1452.
(12) Legrand, M.; McConnell, J. R.; Preunkert, S.; Arienzo, M.; Chellman, N.; Gleason, K.; Sherwen, T.; Evans, M. J.; Carpenter, L. J. Alpine ice evidence of a three-fold increase in atmospheric iodine deposition since 1950 in Europe due to increasing oceanic emissions. *Proc. Natl. Acad. Sci. U.S.A.* **2018**, *115*, 12136−12141.
(13) Zhao, X.; Hou, X.; Zhou, W. Atmospheric Iodine (^{127}I and ^{129}I) Record in Spruce Tree Rings in the Northeast Qinghai-Tibet Plateau. *Environ. Sci. Technol.* **2019**, *53*, 8706−8714.
(14) Caram, C.; Szopa, S.; Cozic, A.; Bekki, S.; Cuevas, C. A.; Saiz-Lopez, A. Sensitivity of tropospheric ozone to halogen chemistry in the chemistry−climate model LMDZ-INCA vNMHC. *Geosci. Model Dev.* **2023**, *16*, 4041−4062.
(15) Wu, N.; Ning, A.; Liu, L.; Zu, H.; Liang, D.; Zhang, X. Methanesulfonic acid and iodous acid nucleation: a novel mechanism for marine aerosols. *Phys. Chem. Chem. Phys.* **2023**, *25*, 16745−16752.
(16) Ning, A.; Zhong, J.; Li, L.; Li, H.; Liu, J.; Liu, L.; Liang, Y.; Li, J.; Zhang, X.; Francisco, J. S.; et al. Chemical Implications of Rapid Reactive Absorption of I2O4 at the Air-Water Interface. *J. Am. Chem. Soc.* **2023**, *145*, 10817−10825.
(17) Feng, W.; Plane, J. M. C.; Chipperfield, M. P.; Saiz-Lopez, A.; Booth, J.-P. Potential Stratospheric Ozone Depletion Due To Iodine Injection From Small Satellites. *Geophys. Res. Lett.* **2023**, *50*, No. e2022GL102300.
(18) Frederiks, N. C.; Heaney, D. D.; Kreinbihl, J. J.; Johnson, C. J. The Competition between Hydrogen, Halogen, and Covalent Bonding in Atmospherically Relevant Ammonium Iodate Clusters. *J. Am. Chem. Soc.* **2023**, *145*, 1165−1175.
(19) Wan, Y.; Huang, X.; Xing, C.; Wang, Q.; Ge, X.; Yu, H. Chemical characterization of organic compounds involved in iodine-initiated new particle formation from coastal macroalgal emission. *Atmos. Chem. Phys.* **2022**, *22*, 15413−15423.
(20) Mondal, K.; Rajakumar, B. Kinetics of IO radicals with C1, C2 aliphatic alcohols in tropospherically relevant conditions. *Environ. Sci. Pollut. Res.* **2023**, *30*, 22590−22605.
(21) Fang, M.; Zhao, X.; Liu, Y.; Shao, Y.; Chen, N.; Luo, M.; Zhang, L.; Liu, Q.; Ma, L.; Xu, D.; et al. Occurrence, evolution and degradation of heavy haze events in Beijing traced by iodine-127 and iodine-129 in aerosols. *Chin. Chem. Lett.* **2022**, *33*, 3507−3515.
(22) Zhang, S.; Li, S.; Ning, A.; Liu, L.; Zhang, X. Iodous acid − a more efficient nucleation precursor than iodic acid. *Phys. Chem. Chem. Phys.* **2022**, *24*, 13651−13660.
(23) Wang, L.; Yan, J.; Saiz-Lopez, A.; Jiang, B.; Yue, F.; Yu, X.; Xie, Z. Mixing state and distribution of iodine-containing particles in Arctic Ocean during summertime. *Sci. Total Environ.* **2022**, *834*, No. 155030.
(24) Liang, Y.; Rong, H.; Liu, L.; Zhang, S.; Zhang, X.; Xu, W. Gas-phase catalytic hydration of I2O5 in the polluted coastal regions: Reaction mechanisms and atmospheric implications. *J. Environ. Sci.* **2022**, *114*, 412−421.
(25) Li, Q.; Tham, Y. J.; Fernandez, R. P.; He, X.-C.; Cuevas, C. A.; Saiz-Lopez, A. Role of Iodine Recycling on Sea-Salt Aerosols in the Global Marine Boundary Layer. *Geophys. Res. Lett.* **2022**, *49*, No. e2021GL097567.
(26) Carpenter, L. J.; Chance, R. J.; Sherwen, T.; Adams, T. J.; Ball, S. M.; Evans, M. J.; Hepach, H.; Hollis, L. D. J.; Hughes, C.; Jickells, T. D.; et al. Marine iodine emissions in a changing world. *Proc. R. Soc. A* **2021**, *477*, 20200824.
(27) Muhire, C.; Tesfay Reda, A.; Zhang, D.; Xu, X.; Cui, C. An overview on metal Oxide-based materials for iodine capture and storage. *Chem. Eng. J.* **2022**, *431*, No. 133816.
(28) Cuevas, C. A.; Fernandez, R. P.; Kinnison, D. E.; Li, Q.; Lamarque, J.-F.; Trabelsi, T.; Francisco, J. S.; Solomon, S.; Saiz-Lopez, A. The influence of iodine on the Antarctic stratospheric ozone hole. *Proc. Natl. Acad. Sci. U.S.A.* **2022**, *119*, No. e2110864119.
(29) Karagodin-Doyennel, A.; Rozanov, E.; Sukhodolov, T.; Egorova, T.; Saiz-Lopez, A.; Cuevas, C. A.; Fernandez, R. P.; Sherwen, T.; Volkamer, R.; Koenig, T. K.; et al. Iodine chemistry in the chemistry−climate model SOCOL-AERv2-I. *Geosci. Model Dev.* **2021**, *14*, 6623−6645.
(30) Wang, M.; He, X.-C.; Finkenzeller, H.; Iyer, S.; Chen, D.; Shen, J.; Simon, M.; Hofbauer, V.; Kirkby, J.; Curtius, J.; et al. Measurement of iodine species and sulfuric acid using bromide chemical ionization mass spectrometers. *Atmos. Meas. Technol.* **2021**, *14*, 4187−4202.
(31) Mahajan, A. S.; Li, Q.; Inamdar, S.; Ram, K.; Badia, A.; Saiz-Lopez, A. Modelling the impacts of iodine chemistry on the northern Indian Ocean marine boundary layer. *Atmos. Chem. Phys.* **2021**, *21*, 8437−8454.
(32) Gómez Martín, J. C.; Saiz-Lopez, A.; Cuevas, C. A.; Fernandez, R. P.; Gilfedder, B.; Weller, R.; Baker, A. R.; Droste, E.; Lai, S. Spatial and Temporal Variability of Iodine in Aerosol. *J. Geophys. Res.: Atmos.* **2021**, *126*, No. e2020JD034410.
(33) Klobas, J. E.; Hansen, J.; Weisenstein, D. K.; Kennedy, R. P.; Wilmouth, D. M. Sensitivity of Iodine-Mediated Stratospheric Ozone Loss Chemistry to Future Chemistry-Climate Scenarios. *Front. Earth. Sci.* **2021**, *9*, No. 617586.
(34) Lewis, T. R.; Gómez Martín, J. C.; Blitz, M. A.; Cuevas, C. A.; Plane, J. M. C.; Saiz-Lopez, A. Determination of the absorption cross sections of higher-order iodine oxides at 355 and 532 nm. *Atmos. Chem. Phys.* **2020**, *20*, 10865−10887.
(35) Rong, H.; Liu, J.; Zhang, Y.; Du, L.; Zhang, X.; Li, Z. Nucleation mechanisms of iodic acid in clean and polluted coastal regions. *Chemosphere* **2020**, *253*, No. 126743.
(36) Kumar, M.; Trabelsi, T.; Gómez Martín, J. C.; Saiz-Lopez, A.; Francisco, J. S. HIO_x−$IONO_2$ Dynamics at the Air−Water Interface: Revealing the Existence of a Halogen Bond at the Atmospheric Aerosol Surface. *J. Am. Chem. Soc.* **2020**, *142*, 12467−12477.
(37) Moreno, C.; Baeza-Romero, M.-T.; Sanz, M.; Gálvez, O.; López Arza, V.; Ianni, J. C.; Espíldora, E. Iodide conversion to iodate in aqueous and solid aerosols exposed to ozone. *Phys. Chem. Chem. Phys.* **2020**, *22*, 5625−5637.
(38) Hoffmann, E. H.; Tilgner, A.; Vogelsberg, U.; Wolke, R.; Herrmann, H. Near-Explicit Multiphase Modeling of Halogen Chemistry in a Mixed Urban and Maritime Coastal Area. *ACS Earth Space Chem.* **2019**, *3*, 2452−2471.
(39) Fortin, C.; Fèvre-Nollet, V.; Cousin, F.; Lebègue, P.; Louis, F. Box modelling of gas-phase atmospheric iodine chemical reactivity in case of a nuclear accident. *Atmos. Environ.* **2019**, *214*, No. 116838.
(40) Fernandez, R. P.; Carmona-Balea, A.; Cuevas, C. A.; Barrera, J. A.; Kinnison, D. E.; Lamarque, J.-F.; Blaszczak-Boxe, C.; Kim, K.; Choi, W.; Hay, T.; et al. Modeling the Sources and Chemistry of Polar Tropospheric Halogens (Cl, Br, and I) Using the CAM-Chem Global Chemistry-Climate Model. *J. Adv. Model. Earth Syst.* **2019**, *11*, 2259−2289.
(41) Kim, K.; Ju, J.; Kim, B.; Chung, H. Y.; Vetráková, L.; Heger, D.; Saiz-Lopez, A.; Choi, W.; Kim, J. Nitrite-Induced Activation of Iodate into Molecular Iodine in Frozen Solution. *Environ. Sci. Technol.* **2019**, *53*, 4892−4900.
(42) Watanabe, K.; Matsuda, S.; Cuevas, C. A.; Saiz-Lopez, A.; Yabushita, A.; Nakano, Y. Experimental Determination of the Photooxidation of Aqueous I^- − as a Source of Atmospheric I_2. *ACS Earth Space Chem.* **2019**, *3*, 669−679.
(43) Yu, H.; Ren, L.; Huang, X.; Xie, M.; He, J.; Xiao, H. Iodine speciation and size distribution in ambient aerosols at a coastal new particle formation hotspot in China. *Atmos. Chem. Phys.* **2019**, *19*, 4025−4039.
(44) Badia, A.; Reeves, C. E.; Baker, A. R.; Saiz-Lopez, A.; Volkamer, R.; Koenig, T. K.; Apel, E. C.; Hornbrook, R. S.; Carpenter, L. J.; Andrews, S. J.; et al. Importance of reactive halogens in the tropical

https://doi.org/10.1021/acs.jpca.5c04243
J. Phys. Chem. A 2025, 129, 7507−7516

marine atmosphere: a regional modelling study using WRF-Chem. *Atmos. Chem. Phys.* **2019**, *19*, 3161−3189.
(45) Legrand, M.; McConnell, J. R.; Preunkert, S.; Arienzo, M.; Chellman, N.; Gleason, K.; Sherwen, T.; Evans, M. J.; Carpenter, L. J. Alpine ice evidence of a three-fold increase in atmospheric iodine deposition since 1950 in Europe due to increasing oceanic emissions. *Proc. Natl. Acad. Sci. U.S.A.* **2018**, *115*, 12136−12141.
(46) Kumar, M.; Saiz-Lopez, A.; Francisco, J. S. Single-Molecule Catalysis Revealed: Elucidating the Mechanistic Framework for the Formation and Growth of Atmospheric Iodine Oxide Aerosols in Gas-Phase and Aqueous Surface Environments. *J. Am. Chem. Soc.* **2018**, *140*, 14704−14716.
(47) Semeniuk, K.; Dastoor, A. Current state of aerosol nucleation parameterizations for air-quality and climate modeling. *Atmos. Environ.* **2018**, *179*, 77−106.
(48) Raso, A. R. W.; Custard, K. D.; May, N. W.; Tanner, D.; Newburn, M. K.; Walker, L.; Moore, R. J.; Huey, L. G.; Alexander, L.; Shepson, P. B.; et al. Active molecular iodine photochemistry in the Arctic. *Proc. Natl. Acad. Sci. U.S.A.* **2017**, *114*, 10053−10058.
(49) Khanniche, S.; Louis, F.; Cantrel, L.; Černušák, I. Investigation of the Reaction Mechanism and Kinetics of Iodic Acid with OH Radical Using Quantum Chemistry. *ACS Earth Space Chem.* **2017**, *1*, 227−235.
(50) Sherwen, T.; Evans, M. J.; Carpenter, L. J.; Schmidt, J. A.; Mickley, L. J. Halogen chemistry reduces tropospheric O_3 radiative forcing. *Atmos. Chem. Phys.* **2017**, *17*, 1557−1569.
(51) Wei, N.; Hu, C.; Zhou, S.; Ma, Q.; Mikuška, P.; Večeřa, Z.; Gai, Y.; Lin, X.; Gu, X.; Zhao, W.; et al. VUV photoionization aerosol mass spectrometric study on the iodine oxide particles formed from O_3-initiated photooxidation of diiodomethane (CH_2I_2). *RSC Adv.* **2017**, *7*, 56779−56787.
(52) Sherwen, T.; Schmidt, J. A.; Evans, M. J.; Carpenter, L. J.; Großmann, K.; Eastham, S. D.; Jacob, D. J.; Dix, B.; Koenig, T. K.; Sinreich, R.; et al. Global impacts of tropospheric halogens (Cl, Br, I) on oxidants and composition in GEOS-Chem. *Atmos. Chem. Phys.* **2016**, *16*, 12239−12271.
(53) Sherwen, T. M.; Evans, M. J.; Spracklen, D. V.; Carpenter, L. J.; Chance, R.; Baker, A. R.; Schmidt, J. A.; Breider, T. J. Global modeling of tropospheric iodine aerosol. *Geophys. Res. Lett.* **2016**, *43*, 10012−10019.
(54) Sipilä, M.; Sarnela, N.; Jokinen, T.; Henschel, H.; Junninen, H.; Kontkanen, J.; Richters, S.; Kangasluoma, J.; Franchin, A.; Peräkylä, O.; et al. Molecular-scale evidence of aerosol particle formation via sequential addition of HIO_3. *Nature* **2016**, *537*, 532−534.
(55) Sellegri, K.; Pey, J.; Rose, C.; Culot, A.; DeWitt, H. L.; Mas, S.; Schwier, A. N.; Temime-Roussel, B.; Charriere, B.; Saiz-Lopez, A.; et al. Evidence of atmospheric nanoparticle formation from emissions of marine microorganisms. *Geophys. Res. Lett.* **2016**, *43*, 6596−6603.
(56) Sherwen, T.; Evans, M. J.; Carpenter, L. J.; Andrews, S. J.; Lidster, R. T.; Dix, B.; Koenig, T. K.; Sinreich, R.; Ortega, I.; Volkamer, R.; et al. Iodine's impact on tropospheric oxidants: a global model study in GEOS-Chem. *Atmos. Chem. Phys.* **2016**, *16*, 1161−1186.
(57) Saiz-Lopez, A.; Baidar, S.; Cuevas, C. A.; Koenig, T. K.; Fernandez, R. P.; Dix, B.; Kinnison, D. E.; Lamarque, J.-F.; Rodriguez-Lloveras, X.; Campos, T. L.; et al. Injection of iodine to the stratosphere. *Geophys. Res. Lett.* **2015**, *42*, 6852−6859.
(58) Roscoe, H. K.; Jones, A. E.; Brough, N.; Weller, R.; Saiz-Lopez, A.; Mahajan, A. S.; Schoenhardt, A.; Burrows, J. P.; Fleming, Z. L. Particles and iodine compounds in coastal Antarctica. *J. Geophys. Res.* **2015**, *120*, 7144−7156.
(59) Thompson, C. R.; Shepson, P. B.; Liao, J.; Huey, L. G.; Apel, E. C.; Cantrell, C. A.; Flocke, F.; Orlando, J.; Fried, A.; Hall, S. R.; et al. Interactions of bromine, chlorine, and iodine photochemistry during ozone depletions in Barrow, Alaska. *Atmos. Chem. Phys.* **2015**, *15*, 9651−9679.
(60) Prados-Roman, C.; Cuevas, C. A.; Hay, T.; Fernandez, R. P.; Mahajan, A. S.; Royer, S.-J.; Galí, M.; Simó, R.; Dachs, J.; Großmann, K.; et al. Iodine oxide in the global marine boundary layer. *Atmos. Chem. Phys.* **2015**, *15*, 583−593.
(61) Prados-Roman, C.; Cuevas, C. A.; Fernandez, R. P.; Kinnison, D. E.; Lamarque, J.-F.; Saiz-Lopez, A. A negative feedback between anthropogenic ozone pollution and enhanced ocean emissions of iodine. *Atmos. Chem. Phys.* **2015**, *15*, 2215−2224.
(62) Saiz-Lopez, A.; Fernandez, R. P.; Ordóñez, C.; Kinnison, D. E.; Gómez Martín, J. C.; Lamarque, J.-F.; Tilmes, S. Iodine chemistry in the troposphere and its effect on ozone. *Atmos. Chem. Phys.* **2014**, *14*, 13119−13143.
(63) Liss, P. S.; Marandino, C. A.; Dahl, E. E.; Helmig, D.; Hintsa, E. J.; Hughes, C.; Johnson, M. T.; Moore, R. M.; Plane, J. M. C.; Quack, B.; et al. Short-Lived Trace Gases in the Surface Ocean and the Atmosphere. In *Ocean-Atmosphere Interactions of Gases and Particles*; Liss, P. S., Johnson, M. T., Eds.; Springer Earth System Sciences; Springer, 2020; pp 1−54.
(64) Šulková, K.; Federič, J.; Louis, F.; Cantrel, L.; Demovič, L.; Černušák, I. Thermochemistry of small iodine species. *Phys. Scr.* **2013**, *88*, No. 058304.
(65) Truesdale, V. W.; Žic, V.; Garnier, C.; Cukrov, N. Circumstantial evidence in support of org-I as a component of the marine aerosol arising from a study of marine foams. *Estuarine, Coastal Shelf Sci.* **2012**, *115*, 388−398.
(66) Saunders, R. W.; Kumar, R.; MacDonald, S. M.; Plane, J. M. C. Insights into the Photochemical Transformation of Iodine in Aqueous Systems: Humic Acid Photosensitized Reduction of Iodate. *Environ. Sci. Technol.* **2012**, *46*, 11854−11861.
(67) Saiz-Lopez, A.; Plane, J. M. C.; Mahajan, A. S.; Anderson, P. S.; Bauguitte, S. J.-B.; Jones, A. E.; Roscoe, H. K.; Salmon, R. A.; Bloss, W. J.; Lee, J. D.; Heard, D. E. On the vertical distribution of boundary layer halogens over coastal Antarctica: implications for O_3, HO_x, NO_x and the Hg lifetime. *Atmos. Chem. Phys.* **2008**, *8*, 887−900.
(68) Saunders, R. W.; Plane, J. M. C. Formation Pathways and Composition of Iodine Oxide Ultra-Fine Particles. *Environ. Chem.* **2005**, *2*, 299−303.
(69) Saunders, R. W.; Kumar, R.; Goméz Martín, J. C.; Mahajan, A. S.; Murray, B. J.; Plane, J. M. C. Studies of the Formation and Growth of Aerosol from Molecular Iodine Precursor. *Z. Phys. Chem.* **2010**, *224*, 1095−1117.
(70) O'Dowd, C. D.; Jimenez, J. L.; Bahreini, R.; Flagan, R. C.; Seinfeld, J. H.; Hämeri, K.; Pirjola, L.; Kulmala, M.; Jennings, S. G.; Hoffmann, T. Marine aerosol formation from biogenic iodine emissions. *Nature* **2002**, *417*, 632−636.
(71) Saiz-Lopez, A.; Plane, J. M. C.; McFiggans, G.; Williams, P. I.; Ball, S. M.; Bitter, M.; Jones, R. L.; Hongwei, C.; Hoffmann, T. Modelling molecular iodine emissions in a coastal marine environment: the link to new particle formation. *Atmos. Chem. Phys.* **2006**, *6*, 883−895.
(72) Pechtl, S.; Lovejoy, E. R.; Burkholder, J. B.; von Glasow, R. Modeling the possible role of iodine oxides in atmospheric new particle formation. *Atmos. Chem. Phys.* **2006**, *6*, 505−523.
(73) Mahajan, A. S.; Plane, J. M. C.; Oetjen, H.; Mendes, L.; Saunders, R. W.; Saiz-Lopez, A.; Jones, C. E.; Carpenter, L. J.; McFiggans, G. B. Measurement and modelling of tropospheric reactive halogen species over the tropical Atlantic Ocean. *Atmos. Chem. Phys.* **2010**, *10*, 4611−4624.
(74) Plane, J. M. C.; Joseph, D. M.; Allan, B. J.; Ashworth, S. H.; Francisco, J. S. An Experimental and Theoretical Study of the Reactions OIO + NO and OIO + OH. *J. Phys. Chem. A* **2006**, *110*, 93−100.
(75) Ball, S. M.; Hollingsworth, A. M.; Humbles, J.; Leblanc, C.; Potin, P.; McFiggans, G. Spectroscopic studies of molecular iodine emitted into the gas phase by seaweed. *Atmos. Chem. Phys.* **2010**, *10*, 6237−6254.
(76) Bloss, W. J.; Rowley, D. M.; Cox, R. A.; Jones, R. L. Kinetics and Products of the IO Self-Reaction. *J. Phys. Chem. A* **2001**, *105*, 7840−7854.
(77) Spietz, P.; Gómez Martín, J. C.; Burrows, J. P. Spectroscopic studies of the I_2/O_3 photochemistry: Part 2. Improved spectra of

https://doi.org/10.1021/acs.jpca.5c04243
J. Phys. Chem. A 2025, 129, 7507−7516

iodine oxides and analysis of the IO absorption spectrum. *J. Photochem. Photobiol.* **2005**, *176*, 50−67.
(78) Harwood, M. H.; Burkholder, J. B.; Hunter, M.; Fox, R. W.; Ravishankara, A. R. Absorption Cross Sections and Self-Reaction Kinetics of the IO Radical. *J. Phys. Chem. A* **1997**, *101*, 853−863.
(79) Gómez Martín, J. C.; Spietz, P.; Burrows, J. P. Spectroscopic studies of the I_2/O_3 photochemistry: Part 1: Determination of the absolute absorption cross sections of iodine oxides of atmospheric relevance. *J. Photochem. Photobiol., A* **2005**, *176*, 15−38.
(80) Schönhardt, A.; Begoin, M.; Richter, A.; Wittrock, F.; Kaleschke, L.; Gómez Martín, J. C.; Burrows, J. P. Simultaneous satellite observations of IO and BrO over Antarctica. *Atmos. Chem. Phys.* **2012**, *12*, 6565−6580.
(81) Furneaux, K. L.; Whalley, L. K.; Heard, D. E.; Atkinson, H. M.; Bloss, W. J.; Flynn, M. J.; Gallagher, M. W.; Ingham, T.; Kramer, L.; Lee, J. D.; et al. Measurements of iodine monoxide at a semi polluted coastal location. *Atmos. Chem. Phys.* **2010**, *10*, 3645−3663.
(82) Commane, R.; Seitz, K.; Bale, C. S. E.; Bloss, W. J.; Buxmann, J.; Ingham, T.; Platt, U.; Pöhler, D.; Heard, D. E. Iodine monoxide at a clean marine coastal site: observations of high frequency variations and inhomogeneous distributions. *Atmos. Chem. Phys.* **2011**, *11*, 6721−6733.
(83) Butz, A.; Bosch, H.; Camy-Peyret, C.; Chipperfield, M. P.; Dorf, M.; Kreycy, S.; Kritten, L.; Prados-Roman, C.; Schwarzle, J.; Pfeilsticker, K. Constraints on inorganic gaseous iodine in the tropical upper troposphere and stratosphere inferred from balloon-borne solar occultation observations. *Atmos. Chem. Phys.* **2009**, *9*, 7229−7242.
(84) Gómez Martín, J. C.; Spietz, P.; Burrows, J. P. Kinetic and Mechanistic Studies of the I_2/O_3 Photochemistry. *J. Phys. Chem. A* **2007**, *111*, 306−320.
(85) Gómez Martín, J. C.; Plane, J. M. C. Determination of the O−IO bond dissociation energy by photofragment excitation spectroscopy. *Chem. Phys. Lett.* **2009**, *474*, 79−83.
(86) Joseph, D. M.; Ashworth, S. H.; Plane, J. M. C. The absorption cross-section and photochemistry of OIO. *J. Photochem. Photobiol.* **2005**, *176*, 68−77.
(87) Huang, R. J.; Seitz, K.; Neary, T.; O'Dowd, C. D.; Platt, U.; Hoffmann, T. Observations of high concentrations of I_2 and IO in coastal air supporting iodine-oxide driven coastal new particle formation. *Geophys. Res. Lett.* **2010**, *37*, L03803.
(88) Pirjola, L.; O'Dowd, C. D.; Yoon, Y. J.; Sellegri, K. Modelling Iodine Particle Formation and Growth from Seaweed in a Chamber. *Environ. Chem.* **2005**, *2*, 271.
(89) Kaltsoyannis, N.; Plane, J. M. C. Quantum chemical calculations on a selection of iodine-containing species (IO, OIO, INO_3, $(IO)_2$, I_2O_3, I_2O_4 and I_2O_5) of importance in the atmosphere. *Phys. Chem. Chem. Phys.* **2008**, *10*, 1723−1733.
(90) Gálvez, O.; Gómez Martín, J. C.; Gómez, P. C.; Saiz-Lopez, A.; Pacios, L. F. A theoretical study on the formation of iodine oxide aggregates and monohydrates. *Phys. Chem. Chem. Phys.* **2013**, *15*, 15572−15583.
(91) Gómez Martín, J. C.; Gálvez, O.; Baeza-Romero, M. T.; Ingham, T.; Plane, J. M. C.; Blitz, M. A. On the mechanism of iodine oxide particle formation. *Phys. Chem. Chem. Phys.* **2013**, *15*, 15612−15622.
(92) Gómez Martín, J. C.; Lewis, T. R.; Blitz, M. A.; Plane, J. M. C.; Kumar, M.; Francisco, J. S.; Saiz-Lopez, A. A gas-to-particle conversion mechanism helps to explain atmospheric particle formation through clustering of iodine oxides. *Nat. Commun.* **2020**, *11*, No. 4521.
(93) Ning, A.; Li, J.; Du, L.; Yang, X.; Liu, J.; Yang, Z.; Zhong, J.; Saiz-Lopez, A.; Liu, L.; Francisco, J. S.; Zhang, X. Heterogenous Chemistry of I_2O_3 as a Critical Step in Iodine Cycling. *J. Am. Chem. Soc.* **2024**, *146*, 33229−33238.
(94) Engsvang, M.; Wu, H.; Elm, J. Iodine Clusters in the Atmosphere I: Computational Benchmark and Dimer Formation of Oxyacids and Oxides. *ACS Omega* **2024**, *9*, 31521−31532.
(95) Hartree, D. R. The Wave Mechanics of an Atom with a Non-Coulomb Central Field. Part I. Theory and Methods. *Math. Proc. Cambridge Philos. Soc.* **1928**, *24*, 89−110.
(96) Fock, V. Näherungsmethode zur Lösung des quantenmechanischen Mehrkörperproblems. *Z. Phys.* **1930**, *61*, 126−148.
(97) Hall, G. G. The molecular orbital theory of chemical valency VIII. A method of calculating ionization potentials. *Proc. R. Soc. London, Ser. A* **1951**, *205*, 541−552.
(98) Roothaan, C. C. J. Self-Consistent Field Theory for Open Shells of Electronic Systems. *Rev. Mod. Phys.* **1960**, *32*, 179−185.
(99) Bartlett, R. J. Many-Body Perturbation Theory and Coupled Cluster Theory for Electron Correlation in Molecules. *Annu. Rev. Phys. Chem.* **1981**, *32*, 359−401.
(100) Bartlett, R. J. Coupled-cluster approach to molecular structure and spectra: a step toward predictive quantum chemistry. *J. Phys. Chem.* **1989**, *93*, 1697−1708.
(101) Bartlett, R. J.; Stanton, J. F. Applications of Post-Hartree−Fock Methods: A Tutorial. *Rev. Comput. Chem.* **1994**, *5*, 65−169.
(102) Crawford, T. D.; Schaefer, H. F., III. *Rev. Comput. Chem.* **2000**, *14*, 33−136.
(103) Čížek, J. On the Correlation Problem in Atomic and Molecular Systems. Calculation of Wavefunction Components in Ursell-Type Expansion Using Quantum-Field Theoretical Methods. *J. Chem. Phys.* **1966**, *45*, 4256−4266.
(104) Čížek, J. On the Use of the Cluster Expansion and the Technique of Diagrams in Calculations of Correlation Effects in Atoms and Molecules. *Adv. Chem. Phys.* **1969**, *14*, 35−89.
(105) Purvis, G. D., III; Bartlett, R. J. A full coupled-cluster singles and doubles model: The inclusion of disconnected triples. *J. Chem. Phys.* **1982**, *76*, 1910−1918.
(106) Raghavachari, K.; Trucks, G. W.; Pople, J. A.; Head-Gordon, M. A fifth-order perturbation comparison of electron correlation theories. *Chem. Phys. Lett.* **1989**, *157*, 479−483.
(107) Bartlett, R. J.; Watts, J. D.; Kucharski, S. A.; Noga, J. Non-iterative fifth-order triple and quadruple excitation energy corrections in correlated methods. *Chem. Phys. Lett.* **1990**, *165*, 513−522.
(108) Stanton, J. F. Why CCSD(T) works: a different perspective. *Chem. Phys. Lett.* **1997**, *281*, 130−134.
(109) Zhao, Y.; Truhlar, D. G. The M06 suite of density functionals for main group thermochemistry, thermochemical kinetics, noncovalent interactions, excited states, and transition elements: two new functionals and systematic testing of four M06-class functionals and 12 other functionals. *Theor. Chem. Acc.* **2008**, *120*, 215−241.
(110) Perdew, J. P.; Chevary, J. A.; Vosko, S. H.; Jackson, K. A.; Pederson, M. R.; Singh, D. J.; Fiolhais, C. Atoms, molecules, solids, and surfaces: Applications of the generalized gradient approximation for exchange and correlation. *Phys. Rev. B* **1992**, *46*, 6671−6687.
(111) Chai, J.-D.; Head-Gordon, M. Long-range corrected hybrid density functionals with damped atom−atom dispersion corrections. *Phys. Chem. Chem. Phys.* **2008**, *10*, 6615−6620.
(112) Stephens, P. J.; Devlin, F. J.; Chabalowski, C. F.; Frisch, M. J. Ab Initio Calculation of Vibrational Absorption and Circular Dichroism Spectra Using Density Functional Force Fields. *J. Phys. Chem.* **1994**, *98*, 11623−11627.
(113) Pritchard, B. P.; Altarawy, D.; Didier, B.; Gibson, T. D.; Windus, T. L. New Basis Set Exchange: An Open, Up-to-Date Resource for the Molecular Sciences Community. *J. Chem. Inf. Model.* **2019**, *59*, 4814−4820.
(114) Feller, D. The role of databases in support of computational chemistry calculations. *J. Comput. Chem.* **1996**, *17*, 1571−1586.
(115) Schuchardt, K. L.; Didier, B. T.; Elsethagen, T.; Sun, L.; Gurumoorthi, V.; Chase, J.; Li, J.; Windus, T. L. Basis Set Exchange: A Community Database for Computational Sciences. *J. Chem. Inf. Model.* **2007**, *47*, 1045−1052.
(116) Dunning, T. H., Jr Gaussian basis sets for use in correlated molecular calculations. I. The atoms boron through neon and hydrogen. *J. Chem. Phys.* **1989**, *90*, 1007−1023.

https://doi.org/10.1021/acs.jpca.5c04243
J. Phys. Chem. A 2025, 129, 7507−7516

(117) Woon, D. E.; Dunning, T. H., Jr Gaussian basis sets for use in correlated molecular calculations. V. Core-valence basis sets for boron through neon. *J. Chem. Phys.* **1995**, *103*, 4572−4585.
(118) Peterson, K. A.; Shepler, B. C.; Figgen, D.; Stoll, H. On the Spectroscopic and Thermochemical Properties of ClO, BrO, IO, and Their Anions. *J. Phys. Chem. A* **2006**, *110*, 13877−13883.
(119) Peterson, K. A.; Figgen, D.; Goll, E.; Stoll, H.; Dolg, M. Systematically convergent basis sets with relativistic pseudopotentials. II. Small-core pseudopotentials and correlation consistent basis sets for the post-d group 16−18 elements. *J. Chem. Phys.* **2003**, *119*, 11113−11123.
(120) Kendall, R. A.; Dunning, T. H., Jr.; Harrison, R. J. Electron affinities of the first-row atoms revisited. Systematic basis sets and wave functions. *J. Chem. Phys.* **1992**, *96*, 6796−6806.
(121) Peterson, K. A.; Yousaf, K. E. Molecular core-valence correlation effects involving the post-d elements Ga−Rn: Benchmarks and new pseudopotential-based correlation consistent basis sets. *J. Chem. Phys.* **2010**, *133*, No. 174116.
(122) Peterson, K. A. A theoretical study of the low-lying electronic states of OIO and the ground states of IOO and OIO. *Mol. Phys.* **2010**, *108*, 393−408.
(123) Stanton, J. F.; Gauss, J.; Cheng, L.; Harding, M. E.; Matthews, D. A.; Szalay, P. G. *CFOUR, Coupled-Cluster Techniques for Computational Chemistry, a Quantum-Chemical Program Package*. http://www.cfour.de.
(124) Smith, D. G. A.; Burns, L. A.; Simmonett, A. C.; Parrish, R. M.; Schieber, M. C.; Galvelis, R.; Kraus, P.; Kruse, H.; Di Remigio, R.; Alenaizan, A.; et al. PSI4 1.4: Open-source software for high-throughput quantum chemistry. *J. Chem. Phys.* **2020**, *152*, No. 184108.
(125) Lehtola, S.; Steigemann, C.; Oliveira, M. J.; Marques, M. A. Recent developments in libxc — A comprehensive library of functionals for density functional theory. *SoftwareX* **2018**, *7*, 1−5.
(126) Almlöf, J.; Faegri, K., Jr.; Korsell, K. Principles for a direct SCF approach to LICAO−MO ab-initio calculations. *J. Comput. Chem.* **1982**, *3*, 385−399.
(127) Van Lenthe, J. H.; Zwaans, R.; Van Dam, H. J. J.; Guest, M. F. Starting SCF calculations by superposition of atomic densities. *J. Comput. Chem.* **2006**, *27*, 926−932.
(128) Franke, P. R.; Stanton, J. F.; Douberly, G. E. How to VPT2: Accurate and Intuitive Simulations of CH Stretching Infrared Spectra Using VPT2+K with Large Effective Hamiltonian Resonance Treatments. *J. Phys. Chem. A* **2021**, *125*, 1301−1324.
(129) East, A. L. L.; Allen, W. D. The heat of formation of NCO. *J. Chem. Phys.* **1993**, *99*, 4638−4650.
(130) Császár, A. G.; Allen, W. D.; Schaefer, H. F. In pursuit of the ab initio limit for conformational energy prototypes. *J. Chem. Phys.* **1998**, *108*, 9751−9764.
(131) Császár, A. G.; Tarczay, G.; Leininger, M. L.; Polyansky, O. L.; Tennyson, J.; Allen, W. D. *Spectroscopy from Space*; Springer: Dordrecht, The Netherlands, 2001; pp 317−339.
(132) Gonzales, J. M.; Allen, W. D.; Schaefer, H. F. Model identity S_N2 reactions $CH_3X + X^-$ (X = F, Cl, CN, OH, SH, NH_2, PH_2): Marcus theory analyzed. *J. Phys. Chem. A* **2005**, *109*, 10613−10628.
(133) Werner, H.-J.; Knowles, P. J.; Celani, P.; Györffy, W.; Hesselmann, A.; Kats, D.; Knizia, G.; Köhn, A.; Korona, T.; Kreplin, D.; et al. *MOLPRO, a Package of Ab Initio Programs*.
(134) Werner, H.-J.; Knowles, P. J.; Manby, F. R.; Black, J. A.; Doll, K.; Heßelmann, A.; Kats, D.; Köhn, A.; Korona, T.; Kreplin, D. A.; et al. The Molpro quantum chemistry package. *J. Chem. Phys.* **2020**, *152*, No. 144107.
(135) Werner, H.-J.; Knowles, P. J.; Knizia, G.; Manby, F. R.; Schütz, M. Molpro: a general-purpose quantum chemistry program package. *Wiley Interdiscip. Rev.: Comput. Mol. Sci.* **2012**, *2*, 242−253.
(136) Noga, J.; Bartlett, R. J. The full CCSDT model for molecular electronic structure. *J. Chem. Phys.* **1987**, *86*, 7041−7050.
(137) Scuseria, G. E.; Schaefer, H. F. A new implementation of the full CCSDT model for molecular electronic structure. *Chem. Phys. Lett.* **1988**, *152*, 382−386.
(138) Watts, J. D.; Bartlett, R. J. The coupled-cluster single, double, and triple excitation model for open-shell single reference functions. *J. Chem. Phys.* **1990**, *93*, 6104−6105.
(139) Bomble, Y. J.; Stanton, J. F.; Kállay, M.; Gauss, J. Coupled-cluster methods including noniterative corrections for quadruple excitations. *J. Chem. Phys.* **2005**, *123*, No. 054101.
(140) Kállay, M.; Gauss, J. Approximate treatment of higher excitations in coupled-cluster theory. *J. Chem. Phys.* **2005**, *123*, No. 214105.
(141) Kállay, M.; Gauss, J. Approximate treatment of higher excitations in coupled-cluster theory. II. Extension to general single-determinant reference functions and improved approaches for the canonical Hartree−Fock case. *J. Chem. Phys.* **2008**, *129*, No. 144101.
(142) Kállay, M.; Nagy, P. R.; Mester, D.; Gyevi-Nagy, L.; Csóka, J.; Szabó, P. B.; Rolik, Z.; Samu, G.; Csontos, J.; Hégely, B.; Ganyecz, A.; Ladjánszki, I.; Szegedy, L.; Ladóczki, B.; Petrov, K.; Farkas, M.; Mezei, P. D.; Horváth, R. A. *MRCC, a Quantum Chemical Program Suite*. www.mrcc.hu.
(143) Mester, D.; Nagy, P. R.; Csóka, J.; Gyevi-Nagy, L.; Szabó, P. B.; Horváth, R. A.; Petrov, K.; Hégely, B.; Ladóczki, B.; Samu, G.; et al. Overview of Developments in the MRCC Program System. *J. Phys. Chem. A* **2025**, *129*, 2086−2107.
(144) Martin, J. M. The eight-valence-electron systems re-examined: convergence of the coupled-cluster series and performance of quasiperturbative methods for quadruple excitations. *Mol. Phys.* **2014**, *112*, 785−793.
(145) Dyall, K. G. Interfacing relativistic and nonrelativistic methods. I. Normalized elimination of the small component in the modified Dirac equation. *J. Chem. Phys.* **1997**, *106*, 9618−9626.
(146) Iliaš, M.; Saue, T. An infinite-order two-component relativistic Hamiltonian by a simple one-step transformation. *J. Chem. Phys.* **2007**, *126*, No. 064102.
(147) Kutzelnigg, W.; Liu, W. Quasirelativistic theory equivalent to fully relativistic theory. *J. Chem. Phys.* **2005**, *123*, No. 241102.
(148) Liu, W.; Peng, D. Exact two-component Hamiltonians revisited. *J. Chem. Phys.* **2009**, *131*, No. 031104.
(149) Sikkema, J.; Visscher, L.; Saue, T.; Iliaš, M. The molecular mean-field approach for correlated relativistic calculations. *J. Chem. Phys.* **2009**, *131*, No. 124116.
(150) Liu, W.; Peng, D. Infinite-order quasirelativistic density functional method based on the exact matrix quasirelativistic theory. *J. Chem. Phys.* **2006**, *125*, No. 044102.
(151) Schoendorff, G.; Boatz, J. A. Relativistic Segmented Correlation Consistent Basis Sets for the 5p and 6p Elements. *J. Phys. Chem. A* **2022**, *126*, 4848−4861.
(152) Bross, D. H.; Peterson, K. A. Correlation consistent, Douglas−Kroll−Hess relativistic basis sets for the 5p and 6p elements. *Theor. Chem. Acc.* **2014**, *133*, No. 1434.
(153) Huang, M.-J.; Watts, J. D. Theoretical Characterization of the F_2O_3 Molecule by Coupled-Cluster Methods. *J. Phys. Chem. A* **2010**, *114*, 10197−10201.
(154) Zhu, R. S.; Lin, M. C. Ab initio studies of ClO_x reactions. VII. Isomers of Cl_2O_3 and their roles in the ClO+OClO reaction. *J. Chem. Phys.* **2003**, *118*, 8645−8655.
(155) Clark, J.; Francisco, J. S. Study of the Stability of Cl_2O_3 Using ab Initio Methods. *J. Phys. Chem. A* **1997**, *101*, 7145−7153.
(156) Pak, C.; Xie, Y.; Schaefer, H. F., III. Properties of Complex Systems: Electron affinities of the dibromine oxides: Br_2O_n (n = 0−4). *Mol. Phys.* **2003**, *101*, 211−225.
(157) Guha, S.; Francisco, J. S. A Density Functional Study of the Equilibrium Structure, Vibrational Spectrum, and Heat of Formation of Br_2O_3. *J. Phys. Chem. A* **1998**, *102*, 6702−6705.
(158) Li, Z.; Jeong, G.-R. Ab initio study for reactions of BrO with BrO, OBrO, and Br_2O_2. *Chem. Phys. Lett.* **2001**, *340*, 194−204.
(159) Elm, J.; Bilde, M.; Mikkelsen, K. V. Assessment of Density Functional Theory in Predicting Structures and Free Energies of Reaction of Atmospheric Prenucleation Clusters. *J. Chem. Theory Comput.* **2012**, *8*, 2071−2077.

https://doi.org/10.1021/acs.jpca.5c04243
J. Phys. Chem. A 2025, 129, 7507−7516